JOURNAL OF MATERIALS SCIENCE 23 (1988) 744–752

Effect of manganese on the oxidation of Fe–Mn–Al–C alloys

C. H. KAO, C. M. WAN
Institute of Materials Science and Engineering, National Tsing Hua University, Hsinchu, Taiwan

The effects of manganese on the oxidation of alloys with the chemical composition (wt%) Fe–5.4Al–1.5Mn–0.58C and Fe–5.3Al–3.5Mn–0.53C at 600, 800 and 1000° C in dry air were investigated. Kinetic curves were determined by thermogravimetric analyses. Optical metallography and electron probe microanalysis were used to examine the oxide scales. The kinetic curves of Fe–5.4Al–1.5Mn–0.58C alloy oxidized at 600, 800 and 1000° C had simple, three- and two-stage parabolic rate laws, respectively. On the other hand, two stages of linear rate law were observed in Fe–5.3Al–3.5Mn–0.53C alloy when oxidized at 600° C, while two distinct parabolic rate laws were found in the same alloy oxidized at 800 and 1000° C. Oxidation behaviours and the oxide formation mechanisms of the alloys at different temperatures are discussed in this paper.

1. Introduction

It is well known that the Fe–Al alloys have excellent high-temperature oxidation resistance due to the formation of a protective layer of alumina during the oxidation process [1–6]. However, the Fe–Al alloys show poor hot workability and high temperature strength which limit their application. During past years, the addition of manganese and/or carbon to the Fe–Al alloys has been used to extend and stabilize the austenite region in alloys to improve both the mechanical properties and hot workability [7–10].

The oxidation behaviour of the Fe–Mn–Al alloy system has been investigated by several researchers [11–16]. Wallwork and co-workers [11, 12] reported that alloys with compositions within the range Fe–5 to 10% Mn–6 to 10% Al develop continuous protective alumina scales and are totally ferritic. They also indicated that the growth of bulky manganese-rich oxides was observed to be more easily achieved in austenite grains, since the manganese content of the austenite region was generally much higher than that of the ferrite phase in duplex alloys. Sauer *et al.* [13] reported that Fe–32Mn–7.5Al–0.6C alloys containing 1 to 2% silicon had good oxidation resistance at 850° C, but not at 1000° C. However, no continuous and protective Al_2O_3 was observed in alloy systems such as Fe–32Mn–Al [13], Fe35Mn–8Al [14] and Fe–30Mn–10Al–1.2Cu–1C [15]. Erhart *et al.* [16] indicated that the oxidation of Fe–30 Mn–10Al–1Si specimens in 10^{-4} atm O_2 leads immediately to the formation of oxide nodules. They also reported that oxidation studies of the same material and surface preparation in air at 800, 900, 1000 and 1100° C showed the formation of a dense, protective Al_2O_3 scale. Obviously, the high partial pressure of oxygen supports the development of a protective alumina scale which in turn gives excellent high-temperature oxidation resistance.

However, the effect of carbon and/or manganese on the oxidation behaviour of the Fe–Al–Mn–C alloys has received little attention [17, 18]. In order to understand the oxidation mechanism of the Fe–Al–Mn–C alloys, a preliminary investigation of the oxidation of simple alloys belonging to the ternary Fe–Al–C alloys was made by us. As described previously [19], the oxidation kinetics of Fe–5.5Al–0.55C alloy after 24 h oxidation at 600, 800 and 1000° C had simple, three- and two-stage parabolic rate laws, respectively. The differences in oxidation behaviour are controlled by the stability of carbide at different oxidation temperatures. Recently, we reported that the oxidation behaviour of Fe–7.5Al–0.65C alloy oxidized for 24 h at 600 to 900° C could be classified into two groups [20]. The change in the oxidation behaviour observed between 600 and 700 to 900° C is related to the effect of temperature on the diffusion of aluminium in the alloy. Internal oxidation occurred beneath the nodules formed on Fe–7.5Al–0.65C alloy after oxidation at 600° C, but no internal oxidation could be observed in specimens of this alloy after 24 h oxidation at 700, 800 and 900° C.

In general, manganese can enter into the formation of spinels of the type (Fe, Mn, Ni)(Fe, Cr, Mn)$_2O_4$, and rhombohedral oxides of (Fe, Mn, Cr)$_2O_3$ in Fe–Ni–Cr alloy systems [21–23]. Possibly, the former might be expected in the inner layers of scales and the latter in outer layers. MnO forms a continuous series of nearly ideal solid solutions with wustite and consequently tends to stabilize this phase as well as spinel. Jackson and Wallwork [24] reported that iron and manganese additions significantly lower the rate of oxidation of the pure metals by reducing the defect concentrations in the oxides and thus the diffusion rates across them.

In other studies by us [25], an austenitic phase was found in the matrix as the maganese concentration

0022–2461/88 $03.00 + .12

reached a certain value in Fe–Al–Mn–C alloys. This is possibly due to an increase of the solubility of carbon in the austenitic phase and to a change of the diffusion rate of elements in the alloy. This means that the appearance of the austenitic phase has an influence on the oxidation behaviour of Fe–Al–Mn–C alloys. The present work was initiated to study the effect of manganese on oxidation resistance by using two-phase Fe–Al–Mn–C alloys with carbide in the ferrite matrix. In addition, the correlation of oxidation behaviour and decarburization occurrence during oxidation was also investigated.

2. Experimental details

Two alloys with different manganese contents were used in this study and the chemical compositions of the alloys are listed in Table I. The alloys were prepared with an air induction furnace under a controlled protective argon atmosphere. The cast ingot was hot-forged at 1200° C from 7 cm to 2.5 cm and then homogenized at 1100° C for 4 h. After surface finishing, the surface and edges of the specimens were mechanically polished with abrasive paper up to 1200 grit. Each specimen was finally cleaned ultrasonically in acetone before the oxidation experiments.

The studies of oxidation kinetics were carried out in the infrared image furnace of an Ulvac/Shink–Uriko thermobalance in dry air with a flow rate of 100 ml min^{-1} and oxidation temperatures of 600, 800 and 1000° C. The heating and cooling rates of the infrared image furnace were 100° C min^{-1}. The oxidation temperature and weight gain curves for each oxidation experiment were recorded by a chart recorder.

The phases present in specimens were identified with X-ray diffraction using a copper target, with a nickel filter and a graphite single-crystal monochromator. The morphology of the oxide scale was examined by optical microscopy. The elemental redistribution and concentration profile in the oxidized specimens were characterized by electron probe microanalysis (EPMA) (Jeol JCXA-733). Quantitative analysis of iron and aluminium was performed with the aid of a ZAF-corrected program. The operation of EPMA was carried out by first raising the voltage to 25 kV with a probe current of 0.03 μA.

3. Experimental results

3.1. Characteristics of alloys before oxidation

Alloy A (Fe–5.4Al–1.5Mn–0.58C) after hot forging and 4 h homogenization at 1100° C was found by X-ray diffraction to be a two-phase material with carbide, $(Fe, Mn)_3AlC_x$, in the ferrite matrix. The lattice parameters were 0.288 and 0.379 nm for ferrite and carbide, respectively. Fig. 1 shows the microstructure for Alloy A in this condition. The dark areas in the micrograph are carbide particles, whereas light areas are the ferrite region. The microstructure of Alloy B (Fe–5.3Al–3.5Mn–0.53C) after heat treatment is similar to that of Alloy A.

TABLE I Chemical compositions of Fe–Mn–Al–C alloys

Alloy	Composition (wt %)			
	Al	Mn	C	Fe
A	5.4	1.5	0.58	Bal.
B	5.3	3.5	0.53	Bal.

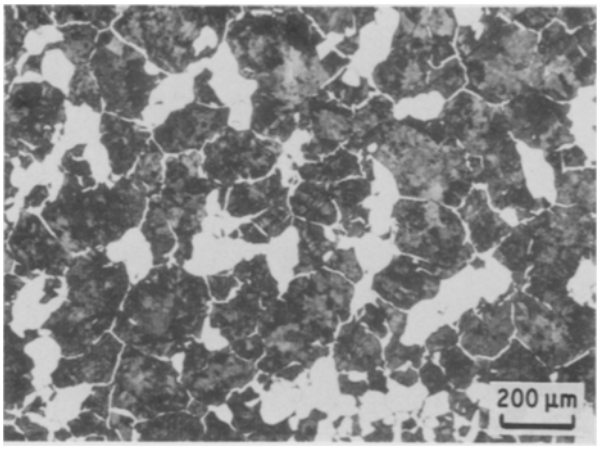

Figure 1 Fe–5.4Al–1.5Mn–0.58C alloy microstructure after heat treatment (4 h at 1100° C).

3.2. Oxidation kinetics

Two Fe–Al–Mn–C alloys with different manganese contents were oxidized at 600° C. The kinetic curves (plots of weight gain per unit area as a function of time) are shown in Fig. 2. The oxidation kinetics obtained from the experiments carried out at 600° C for Alloy A appeared to be different from those for Alloy B. From the square of weight gain per unit area against time, there is a straight-line relationship for Alloy A after oxidation at 600° C (Fig. 3), indicating that the oxidation behaviour follows a simple parabolic rate law at this temperature. The evaluated value of the parabolic constant k_p, is $1.95 \times 10^{-10} g^2 cm^{-4} sec^{-1}$. However, the kinetic results for Alloy B after oxidation at 600° C had two distinct linear rates and the initially linear rate constant (referred to as k_{li}) was lower than the final linear rate constant (k_{lf}) and generally lasted for 16 h. The evaluated values of the linear rate

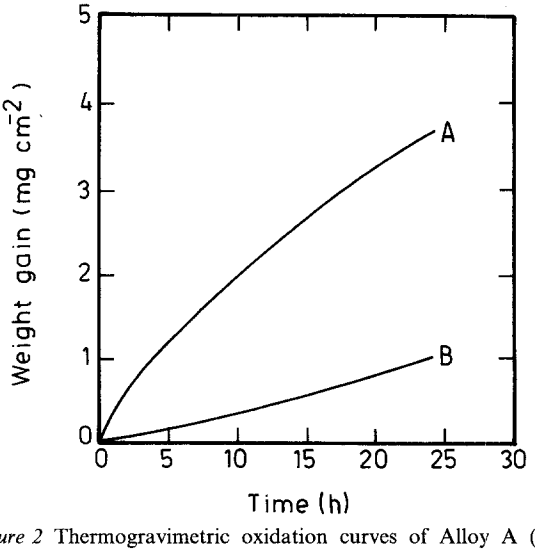

Figure 2 Thermogravimetric oxidation curves of Alloy A (Fe–5.4Al–1.5Mn–0.58C) and Alloy B (Fe–5.3Al–3.5Mn–0.53C) at 600° C.

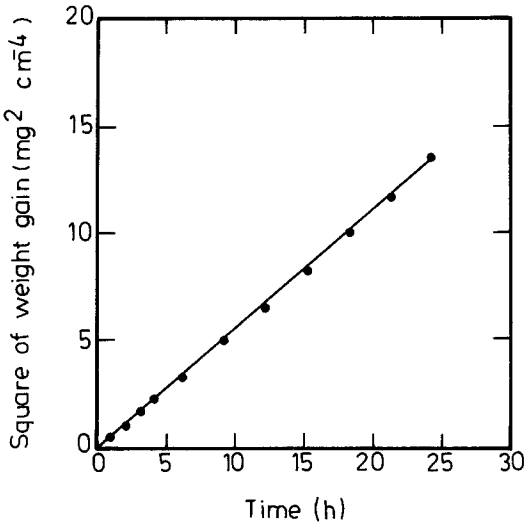

Figure 3 The square of weight gain per unit area against time for Alloy A (Fe–5.4Al–1.5Mn–0.58C) at 600° C.

constant k_{li} is 8.8×10^{12} g cm^{-2} sec^{-1} and k_{lf} is 1.6×10^{-11} g cm^{-2} sec^{-1}.

The oxidation kinetics of Alloys A and B obtained from experiments carried out at 800 and 1000° C, as shown in Fig. 4, appeared to be different from those carried out at 600° C. The square of weight gain per unit area against time, as shown in Fig. 5, indicated two distinct parabolic rates for Alloy A under these conditions, and the final rate constant (referred to as k_{pf}) was higher than the initial parabolic rate constant (k_{pi}). Fig. 5 also showed two distinct parabolic rates for Alloy B after 24 h oxidation at 800° C. In contrast to Alloy A, the initial parabolic rate constant (k_{pi}) is higher than the final parabolic rate constant (k_{pf}). As shown in Figs 6a and b, the kinetic results at 1000° C had two distinct parabolic rates for the Alloys A and B. The initial parabolic rate constant (k_{pi}) was higher than the final parabolic rate constant (k_{pf}) and generally lasted for 3 h under these conditions. All the parabolic rates constants of Alloys A and B after 24 h oxidation at 800 and 1000° C were calculated and are listed in Tables II and III, respectively. The reproducibility of each kinetic curve was checked and the fluctuation was found to be approximately ±4%.

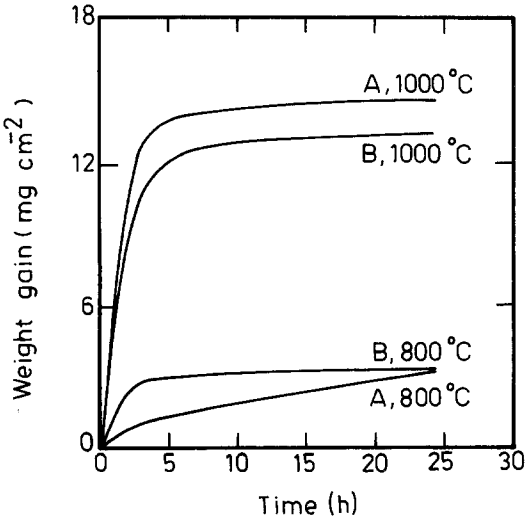

Figure 4 Thermogravimetric oxidation curves of Alloy A (Fe–5.4Al–1.5Mn–0.58C) and Alloy B (Fe–5.3Al–3.5Mn–0.53C) at 800 and 1000° C.

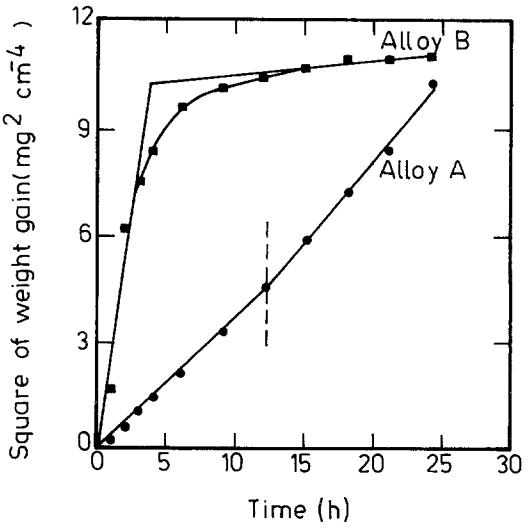

Figure 5 The square of weight gain per unit area against time for Alloy A (Fe–5.4Al–1.5Mn–0.58C) and Alloy B (Fe–5.3Al–3.5Mn–0.53C) at 800° C.

3.3. Analytical aspects

An examination of the cross-section of an oxidized specimen of Alloy A after 24 h oxidation at 600° C is shown in Fig. 7a, which demonstrates two clearly evident oxide layers with a porous exterior. No carbide-free layer and internal oxide could be observed under these conditions. Observation by the X-ray mapping technique showed that there are two oxide layers rich in iron. However, the oxide–matrix interface was found to be rich in aluminium. Fig. 7b shows the concentration of elements in these layers and in the matrix, determined by an electron microprobe with point analysis.

The oxide layers formed on the surface of Alloy B after 10, 24 and 72 h oxidation at 600° C are shown in Figs 8a, b and c, respectively. No decarburized zone could be observed under these conditions. It was observed that oxide crystals first appeared in isolated areas (Fig. 8a) and then spread laterally to meet one another (Figs 8b and c). The internal oxide existing beneath the oxide layer could also be observed. The concentrations of elements in these layers and in the matrix of Alloy B oxidized for 10 and 72 h at 600° C,

TABLE II Parabolic rate constants for Alloys A and B after 24 h oxidation at 800° C

Alloy	Rate constant (g^2 cm^{-4} sec^{-1})	
	k_{pi}	k_{pf}
A	1.05×10^{-10} (0 to 14 h)	1.7×10^{-10} (14 to 24 h)
B	8.6×10^{-10} (0 to 2 h)	9.8×10^{-11} (12 to 24 h)

TABLE III Parabolic rate constants for Alloys A and B after 24 h oxidation at 1000° C

Alloy	Rate constant (g^2 cm^{-4} sec^{-1})	
	k_{pi}	k_{pf}
A	1.5×10^{-8} (0 to 3 h)	7.3×10^{-11} (12 to 24 h)
B	1.05×10^{-8} (0 to 3 h)	1.9×10^{-10} (12 to 24 h)

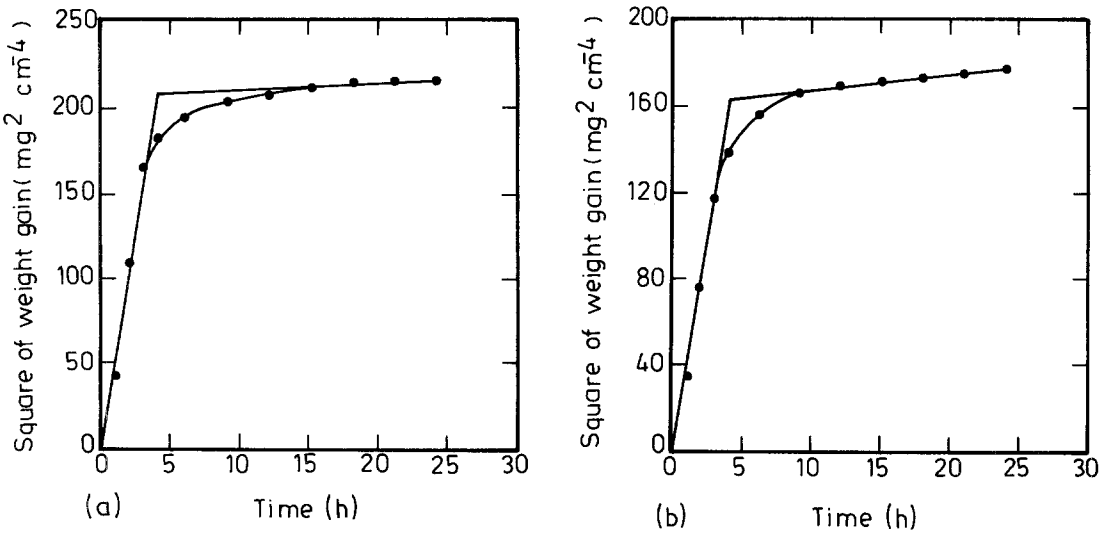

Figure 6 The square of weight gain per unit area against time for (a) Alloy A (Fe–5.4Al–1.5Mn–0.58C) and (b) Alloy B (Fe–5.3Al–3.5Mn–0.53C) at 1000° C.

determined by electron microprobe with point analysis, are shown in Figs 9a and b, respectively. Fig. 9a indicates that the oxide is rich in iron, but the lower region has a relatively higher aluminium concentration of about 10%, together with 3.5% manganese. As the oxidation time gets longer, a continuous oxide layer is formed and the thickness of the layer increases. The concentration profile in Fig. 9b indicates that the element concentrations in the layer are similar to those of the profile in Fig. 9a.

Oxide scales on Alloys A and B after 24 h oxidation at 800° C are shown in Figs 10a and b, respectively. Through optical microstructure investigation, a carbide-free layer could be easily observed along the alloy–scale interfaces of Alloys A and B and the carbide-free zone of Alloy A was larger than that of Alloy B under such conditions. It was also found that the carbide particles in the alloy matrix after oxidation, were different from those before oxidation. No internal oxide could be observed in either alloy under these conditions. Concentration profiles for both alloys after 24 h oxidation at 800° C are shown in Figs 11a and b. The profile in Fig. 11a indicates that there are two oxide layers rich in iron. However, the oxide–matrix interface was found to be rich in aluminium (11.7 wt %) and manganese (2.2 wt %). The metallographic appearance of the cross-sectional area of Alloy B oxidized for 24 h at 800° C indicated that the oxide layers had a porous exterior. Fig. 11b shows that the upper porous oxide was rich in iron, but had negligible amounts of aluminium and manganese. The lower region had a relatively higher aluminium concentration which increased to a value of about 20 wt % in the region close to the alloy–oxide interface. A higher manganese concentration of about 5.8 wt % was also identified in the lower region by EPMA.

Fig. 12 shows that the specimen surface of Alloy A was covered by thick oxide after 4 h oxidation at 1000° C. Through optical investigation, no carbide and no internal oxide could be seen. Fig. 13a shows a scanning electron micrograph of the oxide scale formed after 24 h oxidation at 1000° C. According to the results of X-ray mapping (Figs 13b, c and d) it was found that the outer oxide scale was rich in iron and had a higher aluminium concentration along the

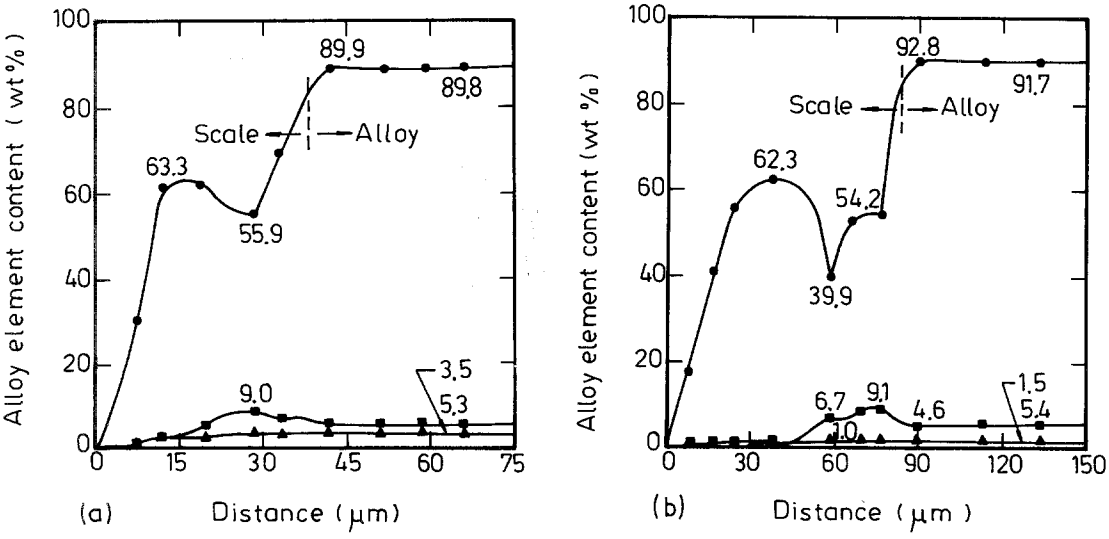

Figure 7 (a) Metallographic cross-section of the oxide scale on Alloy A (Fe–5.4Al–1.5Mn–0.58C) after 24 h at 600° C. (b) The concentration profile across scale and matrix of alloy A oxidized for 24 h: (●) iron, (■) aluminium, (▲) manganese.

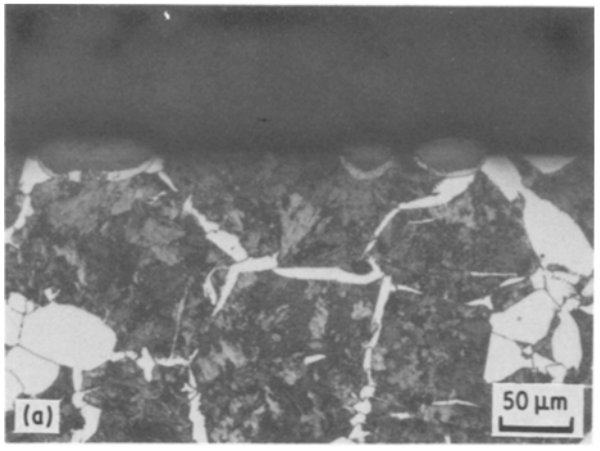

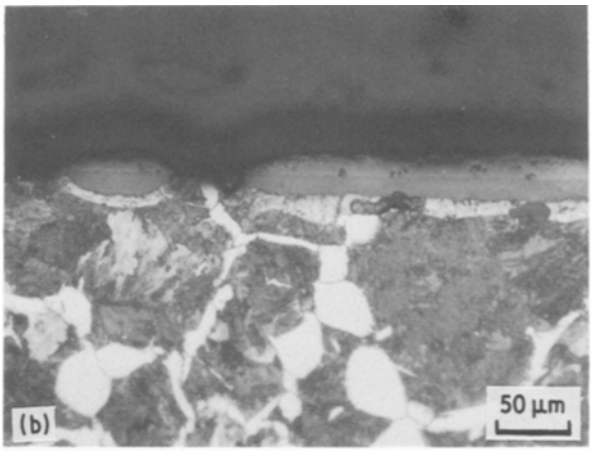

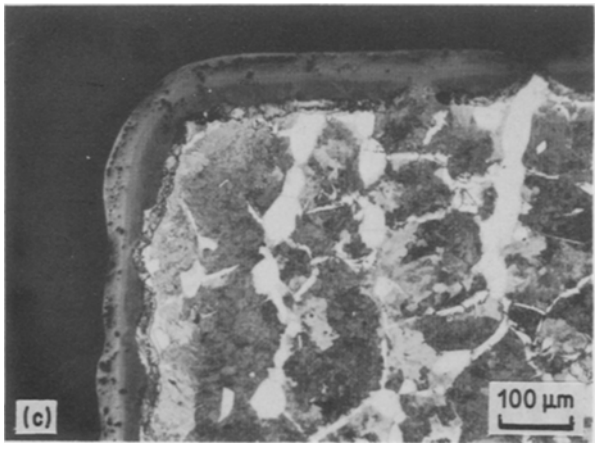

Figure 8 Metallographic cross-sections of the oxide scale on Alloy B (Fe–5.3Al–3.5Mn–0.53C) after (a) 10 h, (b) 24 h and (c) 72 h at 600° C: (●) iron, (■) aluminium, (▲) manganese.

oxide–matrix interface. The cross-section of the oxide scale formed on Alloy B after 24 h oxidation at 1000° C was similar in oxidation behaviour to Alloy A, and no carbides and no internal oxide could be observed. Observations made by X-ray mapping also indicated that the oxide–matrix interface was rich in aluminium.

4. Discussion

According to the results of kinetic studies, the addition of manganese to the alloys used in the present study has little effect at the 1.5% level, but at the 3.5% level there is a considerable difference in the oxidation behaviour in comparison with a previous report for Fe–5.5Al–0.55C alloy by Kao and Wan [19]. This was consistent with the earlier work of Jackson and Wallwork [11], who indicated that the oxidation resistance of Fe–6Al–(1 to 10)Mn alloys increased with increasing manganese concentration. It is interesting, however, to note that different kinds of oxidation behaviour were observed at different manganese contents and different oxidation temperatures.

Fig. 2a indicates that Alloy A (Fe–5.4Al–1.5Mn–0.58C) after 24 h oxidation follows a simple parabolic rate law at 600° C, but two distinct linear rate laws could be observed for Alloy B (Fe–5.3Al–3.5Mn–0.53C) after 24 h oxidation. From the previous studies of Kao and Wan [19], the oxidation of Fe–5.5Al–0.55C alloy at 600° C followed a simple parabolic law. It seems that the addition of 3.5% manganese to Alloy B has a strong effect on the oxidation behaviour at 600° C.

According to the combination of optical morphology, EPMA and X-ray diffraction investigations, the oxide formation mechanism of Fe-5.4Al–1.5Mn–0.58C alloy at 600° C is suggested as follows. The initial stage of oxidation is characterized by the formation of nuclei of FeO, CO (or CO_2) and small

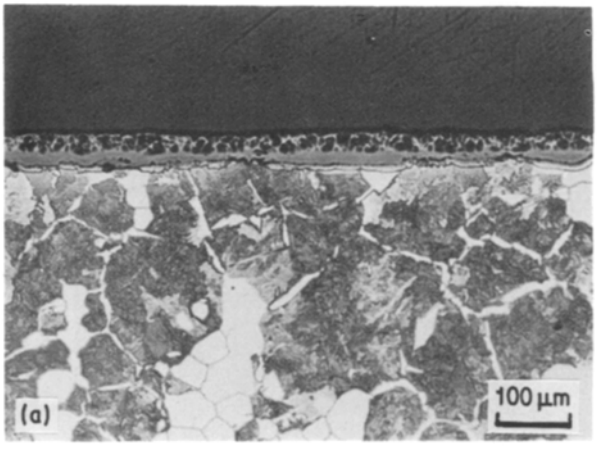

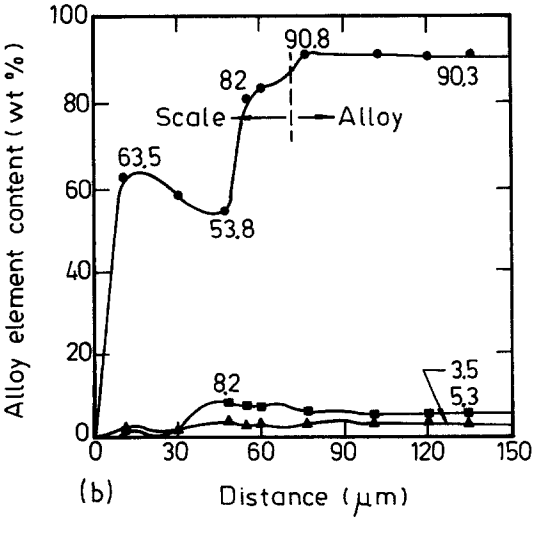

Figure 9 The concentration profile in the layers and matrix of Alloy B oxidized for (a) 24 h and (b) 72 h at 600° C.

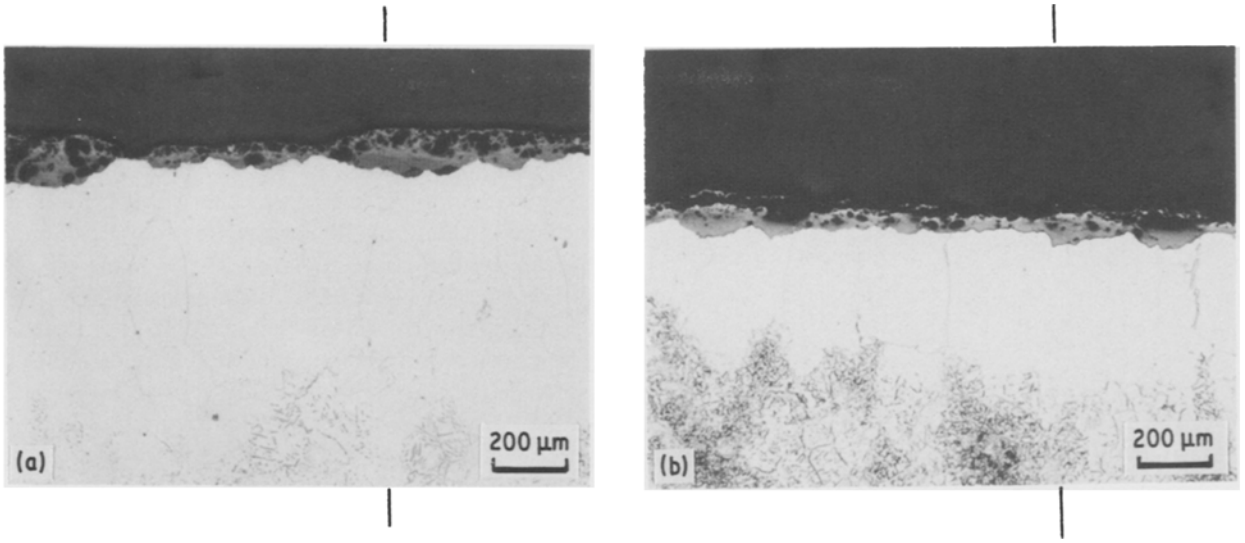

Figure 10 Metallographic cross-sections of the oxide scale on (a) Alloy A (Fe–5.4Al–1.5Mn–0.58C) and (b) Alloy B (Fe–5.3Al–3.5Mn–0.53C) after 24 h at 800° C.

amounts of Al_2O_3 and MnO; CO (or CO_2) gas then evaporates and goes into the environment from the surface of the specimen. As the growth rate of FeO is more rapid than for Al_2O_3 and MnO, this results in iron oxide overgrowing Al_2O_3 and MnO. As the oxidation time gets longer, $Fe_xAl_{2-x}O_4$ (with a small content of oxides of manganese) is suggested to be formed by a chemical reaction between MnO, FeO and Al_2O_3. Generally, CO (or CO_2) gas transports through the pores and microcracks of the oxide scale. The evolution of CO or CO_2 gas always leaves holes in the oxide scale which provide rapid diffusion paths for oxygen ions and apparently interferes with the protective alumina or aluminate [26]. As oxidation proceeds, porous layers with Fe_2O_3 and Fe_3O_4 and no protective layer with $Fe_xAl_{2-x}O_4$ (with a small content of oxides of manganese) are formed at the external and inner layer, respectively, the internal oxides are established beneath the oxide layer.

The oxidation kinetics obtained from experiments carried out at 600° C for Alloy B (Fe–5.5Al–3.5Mn–0.53C) appeared to be different from those of Alloy A (Fe–5.4Al–1.5Mn–0.58C). Two distinct linear rate laws were observed. According to the metallographic studies by optical microscopy, the initial oxidation of Fe–5.3Al–3.5Mn–0.53C alloy at 600° C produces oxide crystals in isolated areas and an internal oxide product beneath the oxide (Fig. 8a). No carbide-free zone can be observed. As the oxidation time gets longer, oxides spread laterally and the thickness of such layers increases. Finally, the oxides meet one another to form a continuous oxide layer (Figs 8b and c), but no protective alumina or aluminate can be found by X-ray diffraction and EPMA techniques. An important question exists: why does the oxide appear at isolated points on the initially oxidized specimen of Fe–5.3Al–3.5Mn–0.53C alloy at 600° C, but not on Fe–5.4Al–1.5Mn–0.58C and Fe–5.5Al–0.55C alloys [19] under the same conditions? Since MnO forms a solid solution with FeO and the defect concentration in the oxide [22], it seems that manganese tends to supress wustite formation in Alloy B oxidized at 600° C. However, because of the lack of quantitative data on diffusion in the various phases formed on

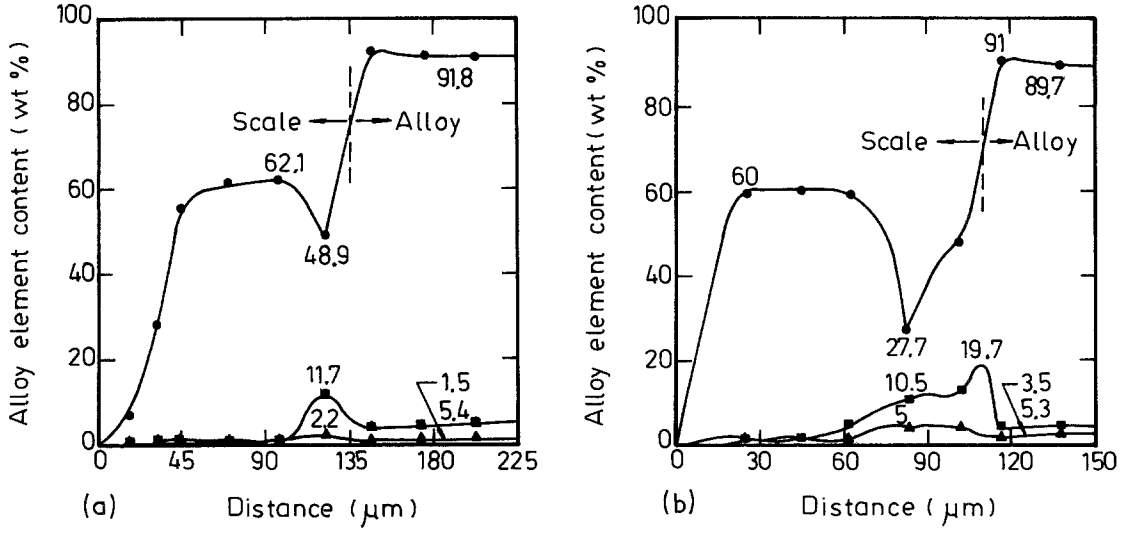

Figure 11 The concentration profile across (a) line marked in Fig. 10a and (b) line marked in Fig. 10b: (●) iron, (■) aluminium, (▲) manganese.

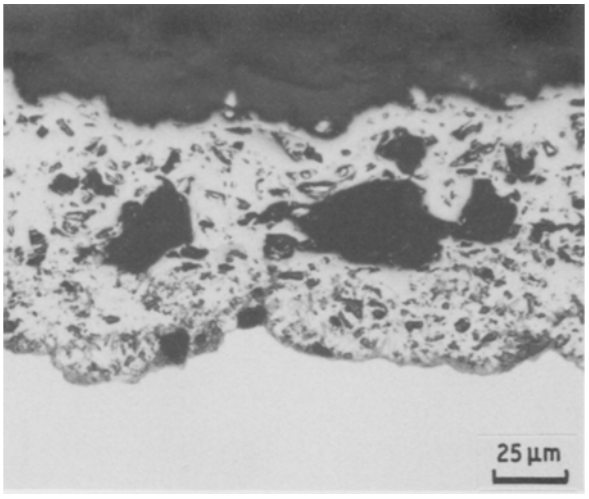

Figure 12 Metallographic cross-section of the oxide scale on Alloy A (Fe–5.4Al–1.5Mn–0.58C) after 4 h at 1000° C.

Fe–Al–Mn–C alloys, a definitive analysis of the oxidation process is not presently possible. Data obtained in this experiment support the following description of the oxidation process.

From the combination of optical morphology, EPMA and X-ray diffraction investigations, the mechanism for oxide nucleation and growth on Alloy B at 600° C could be suggested as follows. The initial stage of oxidation starts with the formation of nuclei of Al_2O_3, FeO, MnO and CO (or CO_2), then CO (or CO_2) evaporates and goes into the environment from the surface of the specimen. In general, MnO forms an ideal solid solution with FeO and consequently tends to stabilize this phase and reduces the defect concentrations in the oxide. This oxidation continues and forms a continuous layer which contains some defects. The defects within the thin film, which become sites of isolated oxide growth, are considered to be the sites of the evaporative positions of CO (or CO_2) or other gases.

With continued oxidation, small isolated oxide particles grow. An outer layer of $(Fe, Mn)_2O_3$ and $MnFe_2O_4$ (with a small content of aluminium oxides) may be established at the base of the isolated oxide. Internal oxide beneath the isolated oxide cannot be suppressed because CO (or CO_2) gas is transported through the scales via pores and microcracks, which provide rapid diffusion channels for oxygen from the environment to the alloy. This suggestion is

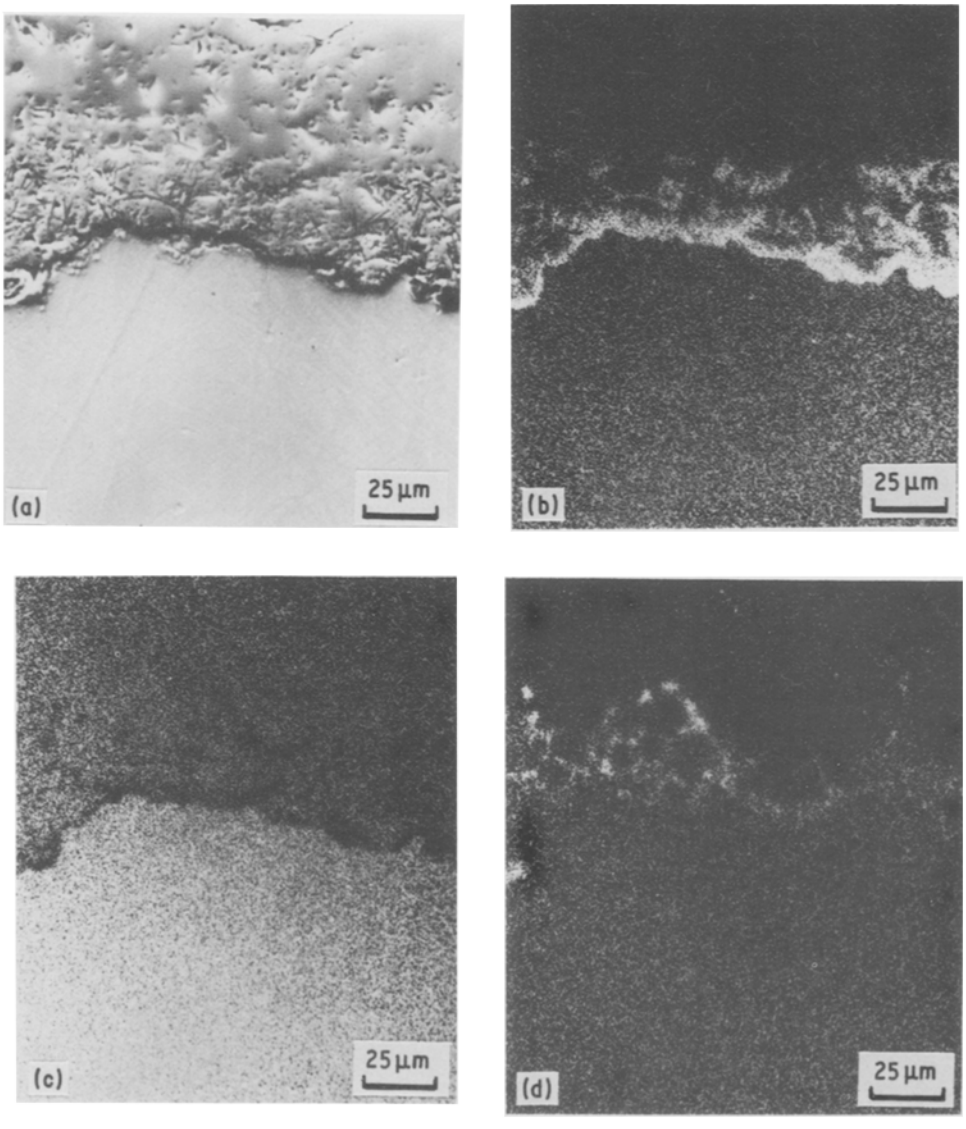

Figure 13 Scanning electron micrograph of the oxide scale on Alloy A (Fe–5.4Al–1.5Mn–0.58C) after 24 h at 1000° C: (a) SEM picture, (b) X-ray map for aluminium, (c) X-ray map for iron, (d) X-ray map for manganese.

confirmed by a previous report by Tomasewica and Wallwork [12]. They indicated that the similar carbon-free alloy Fe–6Al–5Mn develops continuous protective alumina scales and no internal oxide. Anyway, the interface diffusion of both metal and oxygen ions along the metal–$(Fe, Mn)_2O_3$ interface is much higher than at the metal–$MnFe_2O_4$ interface. So, as the oxidation gets longer, an isolated oxide is expanding laterally on the surface, controlled by the phase boundary reaction. As oxidation proceeds, oxides meet one another to form a continuous oxide layer; $(Fe, Mn)_2O_3$ and $MnFe_2O_4$ become the external layer and inner layer, respectively. Internal oxide also occurs beneath the oxide layer on Alloy B.

At 800° C the oxidation kinetics of Alloys A and B appear to be different from that at 600° C. Fig. 5 also indicates that the oxidation behaviour of Alloy A is quite different to that of Alloy B. According to kinetic studies, the initial oxidation rate (k_{pi}) of Alloy A after 24 h at 800° C is lower than the final oxidation rate (k_{pf}). In contrast, the initial oxidation rate (k_{pi}) of Alloy B after 24 h oxidation at 800° C is higher than the final oxidation rate (k_{pf}). From the previous studies by Kao and Wan [19], there are three distinct parabolic rates for the Fe–5.5Al–0.55C alloy after 24 h oxidation at 800° C. This means that the addition of manganese to both the alloys used in the present study has an influence on the oxidation behaviour at 800° C. According to the metallographic studies by optical microscopy, the oxidation of Alloys A and B at 800° C within 24 h was always accompanied by decarburization of the substrate. Under such conditions, a carbide-free layer was generally observed just below the oxide–metal interface and the thickness of the carbide–free layer of Alloy A was higher than that of Alloy B (Figs 10a and b). For a better understanding of the effect of manganese on the formation of this carbide-free layer and the oxidation kinetics, the stability of carbide and the kinetic curve at 800° C were checked for Alloy A at kept 800° C for 60 h. An interesting finding was that no carbide could be found in the matrix, and the oxidation kinetic curves followed three parabolic rate laws after 60 h oxidation. Generally, the first stage of oxidation lasts about 14 h and the second stage lasts from 14 to 44 h, with an oxidation rate value higher than the initial oxidation rate. However, the third oxidation rate is the lowest one among the three distinct parabolic rates law.

These results are similar to those of the previous report for Fe–5.5Al–0.55C alloy by Kao and Wan [19]. The only difference is the time of the distinct oxidation period. This means that the addition of 1.5% manganese to the alloys used in the present study has an influence on the stability of carbide particles. This is confirmed by the microstructure of Alloy B (Fe–5.3Al–3.5Mn–0.53C) after 24 h oxidation at 800° C (Fig. 11b). Under the same conditions, the amount of carbide particles remaining in the matrix of Alloy B is more than that for Alloy A.

The mechanism of oxide growth on Alloy A after 60 h oxidation is similar to that on Fe–5.5Al–0.55C alloy [19]. The deviation of the slope of the kinetic curve of Alloy A might be due to the evolution of a large amount of CO or CO_2 in the secondary stage of oxidation, suggesting that the formation of CO or CO_2 at the alloy–oxide interface may rupture the oxide layer and therefore change the kinetics of the oxidation process. As the oxidation experiment at 800° C is carried out, carbon atoms which mostly come from the decomposition of carbide particles diffuse out to the specimen surface and evaporate with the formation of CO or CO_2. This results in a decrease of the carbon concentration in Alloy A as oxidation continues. When the carbon content falls down to a certain level, evolution of CO (or CO_2) gas is restricted so as to lead to the start of the third stage of oxidation, which always has the lowest rate among the three distinct parabolic rate laws because of the formation of a healing layer at the alloy–oxide interface.

According to the kinetic curve obtained at 800° C, there are two distinct parabolic rates for Alloy B (Fe–5.3Al–3.5Mn–0.53C), indicating that the oxidation behaviour of Alloy B is quite different from that of Alloy A. Such a difference can be explained by the fact that the addition of 3.5% manganese to the alloy enhances the stability of carbide particles in the matrix. Alloy B has a relatively lower dissociation rate of carbide particles and a lower diffusion rate of carbon atoms at this temperature (Fig. 10b). The deviation of the slope where the oxidation behaviour of Alloy B changes from the initial stage to the second stage is related to the formation of aluminate at the oxide–alloy interface that may retard the rate of ionic diffusion and, in turn, change the kinetics of the oxidation process. The results of the present study are confirmed by the EPMA technique (Fig. 11b), which indicates that the lower region of oxide has relatively higher aluminium and manganese concentrations and increases to a value of about 20 wt % Al along the oxide–alloy interface. These results can also explain why large nodules formed on the surface of Fe–5.5Al–0.55C after oxidation at 800° C [19], but not on Fe–5.4Al–1.5Mn–0.58C and Fe–5.3Al–3.5Mn–0.53C alloys under the same conditions.

Kinetic curves obtained from oxidation experiments at 1000° C for Alloys A and B appear to be different from those at 600 and 800° C. They indicate that there are two distinct parabolic laws and a similarity of oxidation behaviour for both alloys at 1000° C. Based on the results of optical observation, carbide was not found in the oxidized specimens of Alloys A and B after three hours of oxidation. It is believed that carbide is not stable under such conditions and that the rate of diffusion of carbon in Alloys A and B at 1000° C is higher than at 800° C. Thus, the specimen surfaces of the alloys are covered by thick scales much more rapidly. Therefore, the formation of aluminate occurred at the final stage and the final oxidation rate dropped.

5. Conclusions

1. During the 24 h oxidation of Alloy A (Fe–5.4Al–1.5Mn–0.58C) at 600° C, a simple parabolic law was observed. There are two distinct linear rates for Alloy B (Fe–5.3Al–3.5Mn–0.53C) at 600° C. No carbide-free layer could be observed in specimens of the alloys

under the same conditions. The differences in oxidation behaviour between Alloys A and B suggested that 3.5% Mn tends to suppress wustite formation on Alloy B.

2. At 800° C, a carbide-free layer could be observed in specimens of the alloys after 24 h oxidation and the stability of carbide particles in the matrix increased with increasing addition of manganese to the alloys. There are three distinct parabolic rates and two distinct parabolic rates for Alloy A after 60 h oxidation and Alloy B after 24 h oxidation at 800° C, respectively.

3. At 1000° C, the addition of manganese to the alloys is not enough to enhance the stability of carbide particles in this study. Carbide quickly dissociated in the matrix, which led to the specimen surfaces of Alloys A and B being covered by thick oxide scales much more rapidly.

Acknowledgement

The authors are pleased to acknowledge the financial support of this research by National Science Council, Republic of China under Grant NSC 75-0201-E007-03.

References

1. E. R. MORGAN and V. F. ZACKAY, *Met. Progr.* **90** (October, 1955) 126.
2. W. E. HAGEL, *Corrosion* **12** (1956) 316.
3. F. SAEGUSA and L. LEE, *ibid.* **22** (1966) 168.
4. T. NAKAYAMA and K. KANEKO, *ibid.* **26** (1970) 187.
5. W. E. BOGGS, *J. Electrochem. Soc.* **118** (1971) 906.
6. P. TOMASEWICA and G. R. WALLWORK, *Oxid. Met.* **19** (1983) 165.
7. D. J. SCHMATZ, *Trans. ASM* **52** (1960) 898.
8. J. L. HAM and R. E. CAIRNS Jr, *Prod. Eng.* **29** (1958) 50.
9. S. K. BANERJI, *Met. Progr.* **113** (1978) 79.
10. J. C. CARCIS, N. ROSAS and K. RIOJA, *ibid.* **117** (1982) 47.
11. P. R. S. JACKSON and G. R. WALLWORK, *Oxid. Met.* **21** (1984) 135.
12. P. TOMASEWICA and G. R. WALLWORK, *Corrosion* **40** (1984) 152.
13. J. P. SAUER, R. A. RAPP, and J. P. HIRTH, *Oxid. Met.* **18** (1982) 285.
14. B. K. LEE, Master's thesis, National Tsing Hua University (1982).
15. C. H. KAO and C. M. WAN, in Proceedings of First CSIR(ROSA)–NSC(ROC) Metal Alloys and Ceramics Workshop, Hsinchu, ROC, 1983, p. 211.
16. H. ERHART, R. WANG and R. A. RAPP, *Oxid. Met.* **21** (1984) 81.
17. C. H. KAO, C. M. WAN and M. T. JAHN, in Proceedings of Conference of the Chinese Society, 1985 Annual meeting for Materials Science, Taipei, ROC, 1985, p 1.
18. *Idem,* in Proceedings of the Annual Meeting of The Metallurgical Society of AIME, New Orleans, March 1986, edited by G. R. Smolik and S. K. Banerji, (TMS Inc., Pennsylvania, USA, 1987) p. 299.
19. C. H. KAO and C. M. WAN, *J. Mater. Sci.* in press.
20. *Idem,*.
21. D. CAPLAN and M. COHEN, *Corrosion* **15** (1959) 141.
22. H. J. YEARIAN, E. C. RANDELL and T. A. LONGO, *ibid.* **12** (1956) 515.
23. *Idem, ibid.* **12** (1956) 561.
24. P. R. A. JACKSON and G. R. WALLWORK, *Oxid. Met.* **20** (1983) 1.
25. C. H. KAO and C. M. WAN, *J. Mater. Sci.*, in press.
26. W. E. BOGGS, *J. Electrochem. Soc.* **118** (1971) 906.

Received 28 May
and accepted 27 July 1987